Desalination and Water Treatment
www.deswater.com

doi: 10.5004/dwt.2022.28376

254 (2022) 302–312
April

On the role of surface functional groups in enhancing Methylene blue adsorption by low-temperature biochar derived from *Platanus orientalis* bark

Weisheng Chen[a], Zhongfang Zhang[a], Hengjia Kang[a], Yujie Guo[a], Tannaz Pak[b], Guoting Li[a,*]

[a]*School of Environmental and Municipal Engineering, North China University of Water Resources and Electric Power, Zhengzhou 450046, China, Tel. +86-371-69127538; Fax: +86-371-65790239; emails: lipsonny@163.com (G. Li), tclbaby@126.com (W. Chen), zf2510722293@163.com (Z. Zhang), k15294916900@163.com (H. Kang), guoyujie@ncwu.edu.cn (Y. Guo)*
[b]*School of Computing, Engineering, and Digital Technologies, Teesside University, Borough Road, Middlesbrough, TS1 3BA, UK, email: t.pak@tees.ac.uk (T. Pak)*

Received 12 August 2021; Accepted 2 March 2022

ABSTRACT

In this study the *Platanus orientalis* bark biochar prepared by pyrolysis under different temperatures was used for adsorptive removal of a dye Methylene blue. Our results show that the biochar adsorption capacity decreases with increasing pyrolysis temperature. However, the Brunauer–Emmett–Teller surface area of the biochar shows little change with increasing pyrolytic temperature. The bark biochar pyrolyzed at 200°C (BC200) outperformed those biochar produced under other pyrolytic temperatures. For both the as-prepared and demineralized BC200 (D-BC200), Elovich kinetic model described the adsorption process better, indicating a chemisorption process in nature. Especially high mesopore content structure within D-BC200 was superior to other demineralized biochar samples. Fourier-transform infrared spectroscopy analysis demonstrated that only the D-BC200 had comparable content of surface functional groups with the raw bark. Boehm titration and X-ray photoelectron spectroscopy analysis indicated the abundant existence of carboxyl acid/ester group. Surface functional groups play a key role in contaminant removal. By Langmuir isotherm model, the q_{max} on the as-prepared BC200 and D-BC200 achieved 199.5 and 237.8 mg/g, respectively. Thermodynamic analysis demonstrates that the adsorption process was spontaneous and endothermic. We measure a higher adsorption enthalpy for D-BC200 which indicates that the process was more sensitive to the change of reaction temperature.

Keywords: Platanus orientalis bark biochar; Adsorption; Methylene blue; Dye; Kinetics; Thermodynamics

1. Introduction

Carbonaceous materials have attracted wide attention in the field of environmental remediation because of their large surface area, high affinity towards organic contaminants, and ease of regeneration (sustainability and cost). In the recent decade, specific attention has been paid to carbon nanotube, graphene, and activated carbon for their use in water and wastewater treatment [1–3]. Activated carbon is known to have first been applied for water treatment by the ancient Egyptians in 2000 B.C.

Despite their high performance, the main drawback for commercial application of these carbonaceous adsorbents at large scale remains the high cost of these materials. For example, activated carbon has become the preferred

* Corresponding author.

adsorptive for removal of organic pollutants in the process of drinking water purification. However, activated carbon is not considered as a cost-effective choice when it comes to wastewater treatment application. Instead, other low-cost carbonaceous adsorbents such as waste biomass are used in practice. However, among other shortfalls use of raw biomass (as opposed to pyrogenic biomass) for water treatment is known to potentially result in organic leaching into soil/groundwater, causing secondary pollution. Therefore, it is well-established that the use of untreated biomass does not provide a sustainable solution to this problem. Instead, low-cost carbonaceous adsorbents (derived from biomass) offer an alternative solution for water and wastewater treatment. Such stable carbonaceous adsorbents are therefore in high demand.

In the past decade, biochar derived from waste biomass has emerged as a promising low-cost adsorbent with the potential for environmental remediation [4]. Biochar is a stable carbon-rich product of biomass carbonization in an oxygen-limited environment. This process is known as pyrolysis. As a multifunctional material, biochar has application in the energy and environment industry. Biochar offers a sustainable solution to mitigating climate change through long-term carbon sequestration while also enabling land remediation, contaminant immobilization, and water purification [4–7]. Biochar is produced from a diverse range of biomass feedstock such as agricultural waste streams, forestry waste, animal manures, and sewage sludge. Similar to activated carbon, biochar is diverse in its structure and properties. Importantly, the existence of surface functional groups in both biochar and activated carbon (i.e., carboxyl, lactonic, and phenolic) facilitates the adsorptive removal of contaminants from aqueous solution. Although activated carbon displays significantly larger surface area compared to biochar, given its relatively lower production cost biochar has become a useful alternative for application at large scale, for example, within the field of water treatment [5,8,9]. Adsorption-based water treatment offers a range of advantages including high efficiency, low cost, ease of operation, and relatively low sensitivity towards other existing substances. This, therefore, makes biochar-based adsorption process an attractive option [10,11].

In biochar production the quantity and quality of biochar is known to be a function of the selected pyrolysis temperature among other factors (e.g., heating rate and residence time). Clearly, biochar produced at low-temperatures is preferred from energy consumption and cost point of view.

With respect to the water treatment capacity of biochar, it is shown that biochar has the potential for catalytic oxidation of organic contaminants in water. Our previous study indicated that bagasse biochar promotes catalytic oxidation of Methylene blue [12]. Further, introduction of polyethylene-polypropylene glycol (F127) as soft-template agent or hydrothermal pretreatment could enhanced adsorption capability of the prepared biochar as well [13,14].

In this research, we investigate the use of *Platanus orientalis* tree bark (a popular landscaping tree in north China) as a biochar feedstock. We measure the efficiency of a range of biochar samples (produced at different temperatures) for adsorptive removal of a typical dye from wastewater. Considering the cost and efficiency, adsorption is considered as one of the most applicable technologies as it is convenient, reliable and cost-effective. Our findings show that an increase in dye uptake occurs with increasing pyrolytic temperature. While this dependency is reported in the literature, the adsorption mechanisms controlling this effect are not explicitly explored and discussed [15–18]. In this contribution, the adsorption performance (adsorption kinetics and isotherm) is systematically investigated for the low-temperature biochar derived from the *Platanus orientalis* tree bark.

2. Materials and methods

2.1. Materials

Methylene blue (mass fraction > 98.5%, chemically pure, MB) was purchased from Tianjin Chemical Reagent Research Institute. The other chemicals used were of analytical grade. Deionised (DI) water was used throughout the study.

2.2. Preparation of Platanus orientalis bark biochar

The *Platanus orientalis* tree bark was collected from Huayuan Campus of North China University of Water Resources and Electric Power located in Zhengzhou, Henan Province. These *Platanus orientalis* trees were planted in the year of 1990 when the campus was established. The collected *Platanus orientalis* bark was washed, dried, crushed, and sieved through a 40 mesh sieve (0.425 mm in size). The biochar preparation procedure is explained in our previous study [19]. Briefly, the bark biochar was prepared in a furnace by pyrolyzing the biomass at a selected temperature for 3 h. The resulting biochar was washed in HCl acid solution (4 M) for 12 h for demineralization of fly ash. Subsequently, the separated biochar was rinsed with DI water until a neutral solution (pH~7) was achieved. The product was then oven-dried overnight at 80°C, and preserved in a desiccator until further use. The *Platanus orientalis* bark biochar (PO-BB) samples pyrolyzed at 200°C, 300°C, 400°C, 500°C and 600°C were hereafter referred to as BC200, BC300, BC400, BC500 and BC600, respectively. The demineralized biochar is indicated as D-BC.

2.3. Characterization

The surface morphology of the raw *Platanus orientalis* bark and biochar was characterized using scanning electron microscopy (Philips Quanta-2000, SEM) coupled with an energy dispersive X-ray (EDX) spectrometer. Biochar surface functional groups were explored using Fourier-transform infrared spectroscopy (Nicolet NEXUS 470, FTIR) with the studied wavelengths ranging from 400 to 4,000 cm^{-1}. The biochar specific surface area was measured using nitrogen-based Brunauer–Emmett–Teller (BET) method (NOVA 2200e). Also, chemical analysis was performed using X-ray photoelectron spectroscopy (ESCALAB 250Xi, XPS) technique. The acidic functional groups (i.e., carboxyl, lactonic, and phenolic) was determined using Boehm's titration method [20,21].

2.4. Batch adsorption studies

A stock solution of MB (500 mg/L) was prepared in DI water. All working solutions were prepared by diluting this stock solution with DI water to the desired concentration. Adsorption of MB onto the PO-BB biochar was performed in a batch experiment. Bark biochar (10 mg) was added to conical flasks containing 50 mL of MB solution (20 mg/L). The mixture was placed in an oscillating shaker operated at 140 rpm for 24 h. For the kinetics study, 200 mg of bark biochar was added to 1,000 mL solution with initial MB concentration of 20 mg/L. The mixed solution was magnetically stirred at a constant rate for 24 h. Samples were collected at different time steps. The adsorption reaction was carried out at 298 K except where the effect of reaction temperature was under study. All solution pH values were maintained at neutral pH except where the effect of pH was under study. Solution pH was adjusted by the addition of dilute HCl or NaOH solutions.

2.5. Analysis methods

After adsorption, samples were collected and filtered through a 0.45 μm syringe membrane before analysis. The concentration of MB was measured using the UV/Vis spectroscopy (mini-spectrophotometer, Shimadzu) technique at the wavelength of 664 nm (absorption peak). The removal percentage of MB was given by:

$$R = \left(1 - \frac{C_t}{C_0}\right) \times 100\% \tag{1}$$

The adsorption capacities (q_e, q_t) were calculated as follows:

$$q_e = \frac{(C_0 - C_e)V}{W} \tag{2}$$

$$q_t = \frac{(C_0 - C_t)V}{W} \tag{3}$$

where q_e and q_t (mg/g) are the adsorption capacities at equilibrium and time t (min); C_0, C_e and C_t (mg/L) are the concentrations of MB at initial stage, equilibrium and a time t (min), respectively; V (L) is the volume of solution, and W (g) is the mass of the PO-BB biochar.

3. Results and discussion

3.1. Effect of pyrolytic temperature on MB adsorption

Increasing pyrolytic temperature can increase the carbon content as well as the thermal stability of the produced biochar. Accordingly, the structural and surface characteristics of biochar can be significantly controlled [22,23]. For both as-prepared and demineralized biochar, MB uptake decreases with increasing pyrolytic temperature dramatically (Fig. 1). Increasing pyrolytic temperature means increased energy cost for biochar production. Meanwhile, as the raw biochar has a high content of fly ash, its adsorption capability is deduced to be altered after HCl treatment. The demineralized biochar displays better adsorption capacity compared to the as-prepared biochar. This can be attributed to the higher carbon content of the demineralized biochar achieved by HCl treatment. As such, we conclude that the increased pyrolytic temperature is not preferred since the low-temperature biochar shows a higher adsorption capability.

3.2. Adsorption kinetics

Based on adsorption kinetics adsorption rate is predicted. Kinetic interactions between the adsorbent and adsorbate can also be studied. The adsorption kinetics for MB uptake onto the as-prepared BC200 and D-BC200 was investigated at pH 3, 5, 7, 9 and 11, as depicted in Fig. 2. Since the two biochar samples have a moderate adsorption

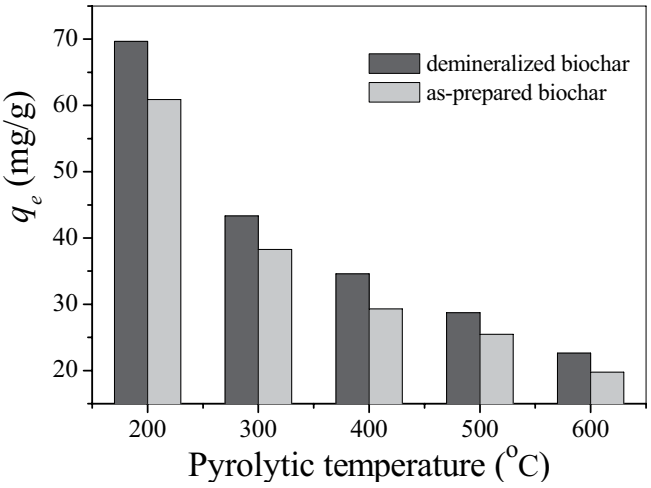

Fig. 1. Effect of pyrolytic temperature on MB adsorption at neutral solution pH.

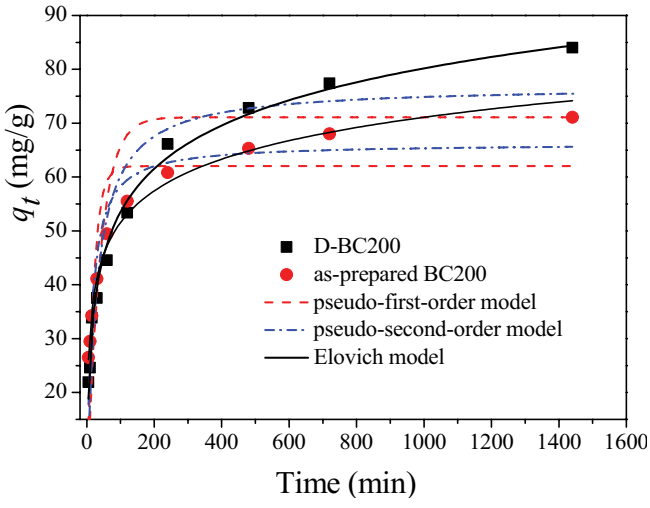

Fig. 2. Simulation of the MB adsorption kinetics on the as-prepared BC200 and D-BC200 using the pseudo-first-order, pseudo-second-order, and Elovich models at pH 7.

capacity for MB at neutral solution pH, only the adsorption kinetics at pH of 7 is presented here. A number of commonly used kinetic models, including the pseudo-first-order (PFO) [24], pseudo-second-order (PSO) [25], and Elovich [26,27] models were employed to fit the experimental data. The calculated kinetic parameters are shown in Table 1.

The PFO and PSO models are nonlinear, they are expressed as Eqs. (4) and (5), respectively:

$$q_t = q_e\left(1 - e^{-k_1 t}\right) \tag{4}$$

$$q_t = \frac{k_2 q_e^2 t}{\left(1 + k_2 q_e t\right)} \tag{5}$$

where q_e and q_t are the adsorption capacities (mg/g) of the as-prepared BC200 and D-BC200 at equilibrium and at time t (min), respectively; k_1 (min^{-1}) and k_2 (g/(mg min)) are the adsorption rate constants for the PFO and PSO models, respectively.

The Elovich model, used to describe chemisorption occurring on a solid-liquid interface, can be written as:

$$q_t = k\ln\left(t\right) + a \tag{6}$$

where k (g/(mg min)) and a (mg/g) are constants.

According to Fig. 2, in our experiment about 80% of the MB adsorption occurs within the initial 6 h. At pH 7, our data show that both the Elovich and PSO kinetic models can better describe the experimental data compared to the pseudo-first-order model, for both the as-prepared BC200 and D-BC200 samples. Literature studies suggest that diffusion accounts for the Elovich kinetic pattern and the rate-determining step can be diffusive in nature [28,29]. From Table 1, most of the correlation coefficients (R^2) of PFO were less than 0.845, while in contrast the R^2 values of the Elovich model are greater than 0.925. The R^2 values for PSO model are all higher than 0.876, making them relatively larger than those of PFO model, and smaller than those derived from Elovich kinetic pattern. As the Elovich kinetic model is known to capture the chemisorption process, this may suggest that chemisorption has occurred between MB molecules and the produced biochar.

3.3. Characterization of PO-BB biochar

Fig. 3 shows SEM images of the biochar samples BC200 and BC600 before and after demineralization treatment. The morphologies of the raw *Platanus orientalis* bark are similar to those of BC200, and only those of BC200 are presented here. These biochar samples display a distinctly irregular structure. Compared to BC200 illustrated in Fig. 3a and b, the biochar BC600 particles became smaller and most of them are within 20 μm. In particular, Fig. 3h shows a more complex porous structure, which enhances the adsorption capability of biochar BC600. Fig. 4 and Table 2 show the outcome of the BET surface area measurements for the biochar samples under study. The D-BC200, D-BC400 and D-BC600 achieved 13.95, 9.18 and 5.28 m^2/g, respectively, with pore sizes of 6.27, 9.07 and 16.11 nm. Actually, the increased pyrolytic temperature did not improve the surface area of biochar while their pore size was significantly enlarged. The above also proved that biochar could be classified as mesoporous material with average pore size in the range of 2~50 nm [30].

Additionally, based on EDS analysis the carbon content (wt.%) of the as-prepared BC200, D-BC200, as-prepared

Table 1
Adsorption kinetic parameters for the kinetic models including pseudo-first-order (PFO), pseudo-second-order (PSO) and Elovich models

Model	Condition	Parameters	pH = 3	pH = 5	pH = 7	pH = 9	pH = 11
PFO	D-BC200	q_e (mg/g)	23.8	60.9	71.1	76.5	89.2
		k_1 (min^{-1})	0.0308	0.0243	0.0257	0.0539	0.0985
		R^2	0.927	0.845	0.766	0.740	0.638
	As-prepared BC200	q_e (mg/g)	22.9	51.6	62.0	69.1	84.6
		k_1 (min^{-1})	0.0257	0.0553	0.0520	0.0749	0.132
		R^2	0.922	0.749	0.770	0.701	0.889
PSO	D-BC200	q_e (mg/g)	25.9	66.0	76.9	81.8	94.3
		k_2 (g/(mg min))	0.00146	5.05×10^{-4}	4.68×10^{-4}	9.16×10^{-4}	1.56×10^{-4}
		R^2	0.963	0.930	0.897	0.898	0.876
	As-prepared BC200	q_e (mg/g)	17.9	55.2	66.2	73.5	88.6
		k_2 (g/(mg min))	0.00125	0.00138	0.00111	0.0014	0.00243
		R^2	0.965	0.911	0.918	0.887	0.901
Elovich	D-BC200	a	–1.647	–0.771	0.185	15.4	36.9
		k	4.23	9.98	11.58	10.52	9.40
		R^2	0.925	0.976	0.988	0.994	0.966
	As-prepared BC200	a	–2.89	10.8	12.5	21.1	44.7
		k	4.24	7.04	8.49	8.49	7.29
		R^2	0.947	0.986	0.985	0.992	0.959

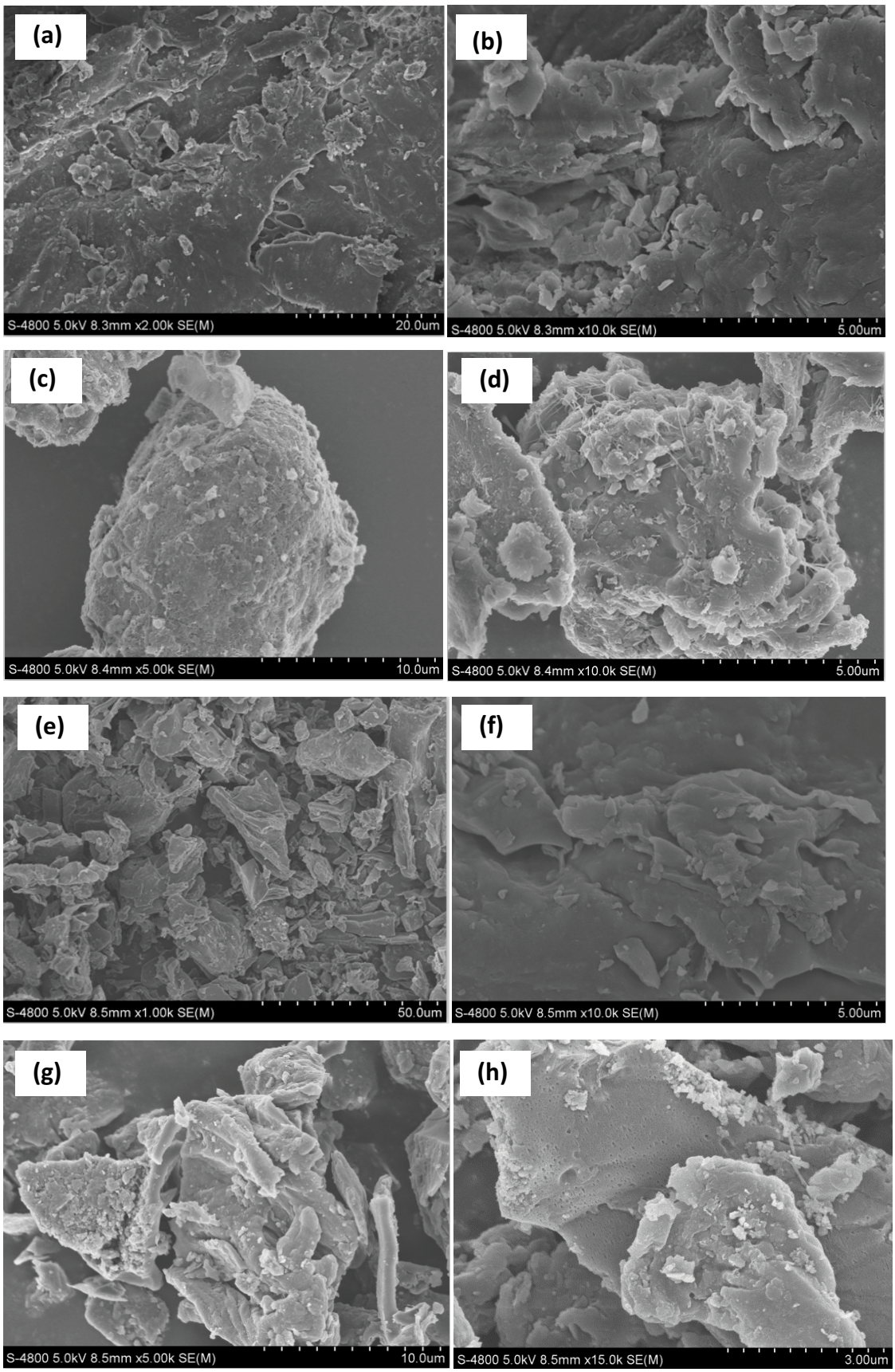

Fig. 3. SEM images of the PO-BB biochar including the D-BC200 (a, b), the raw BC200 (c, d), the D-BC600 (e, f) and the raw BC600 (g, h).

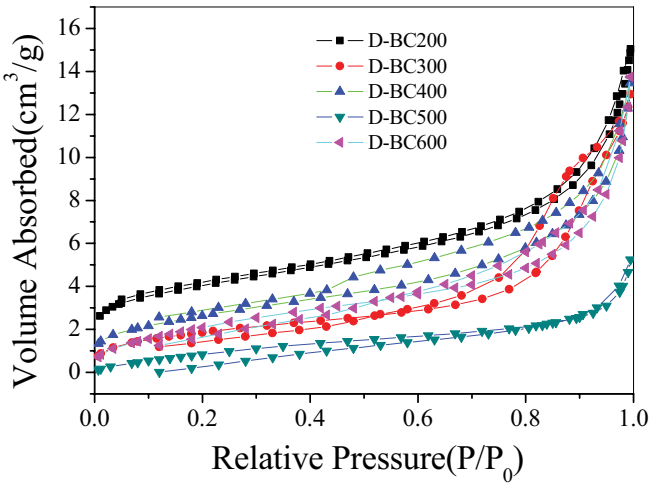

Fig. 4. Sorption isotherm of N_2 onto PO-BB biochar prepared under different pyrolytic temperatures.

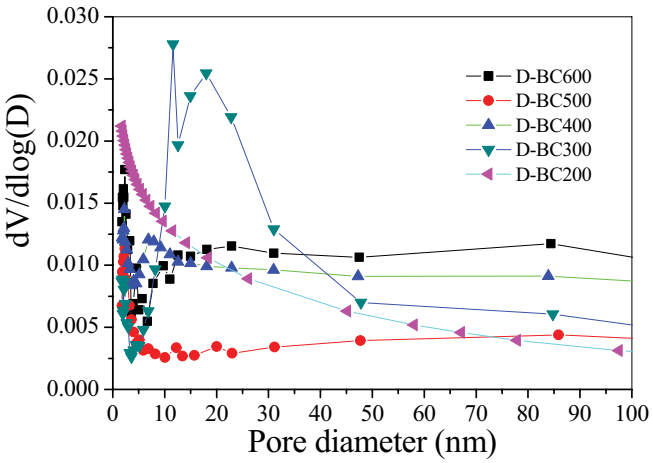

Fig. 5. Pore size distributions of PO-BB biochar by Barrett–Joyner–Halenda method calculating.

Table 2
BET analysis parameters and yield of PO-BB biochar at different pyrolysis temperatures

Sample	S_{BET} (m^2/g)	Pore volume (cm^3/g)	Pore size (nm)	Yield (%)
D-BC200	13.95	0.0219	6.27	98.9
D-BC300	6.59	0.0200	12.15	68.8
D-BC400	9.18	0.0208	9.07	43.8
D-BC500	1.76	0.00811	18.40	30.9
D-BC600	5.28	0.0213	16.11	25.5

BC600 and D-BC600 achieved 33.3%, 59.5%, 76.8% and 86.2%, respectively. These proved the increasing carbon content with an increase in the pyrolytic temperature, and existence of considerable content of carbon on the D-BC200 and D-BC600. At the same time, judged from Fig. 5, the pore size distributions of the biochar D-BC200 was obviously different from those of other demineralized biochar samples. On one hand, a significantly lower micropore distribution structure within D-BC200 was observed compared to other demineralized biochar samples. Comparatively speaking, the macropore content within D-BC200 was slightly lower than most of the other demineralized biochar samples. On the other hand, the especially high mesopore content structure within D-BC200 was superior to other demineralized biochar samples. The amount of specific surface area of mesopore structure within D-BC200 was as much as 88.6% while those of D-BC300, D-BC400, D-BC500, D-BC600 were 82.5%, 87.9%, 86.45% and 80.6%, respectively.

FTIR analysis could reflect the sensitive changes of surface functional groups especially for the oxygen-containing groups on the carbonaceous substrate. The FTIR spectra of the raw bark and demineralized biochar samples prepared under different pyrolytic temperatures are shown in Fig. 6. On one hand, almost all the absorption bands illustrated in Fig. 6 diminished with increasing pyrolytic temperature, indicating the reduction of surface functional groups. The bands at 2,925 cm^{-1} (aliphatic C–H stretching)

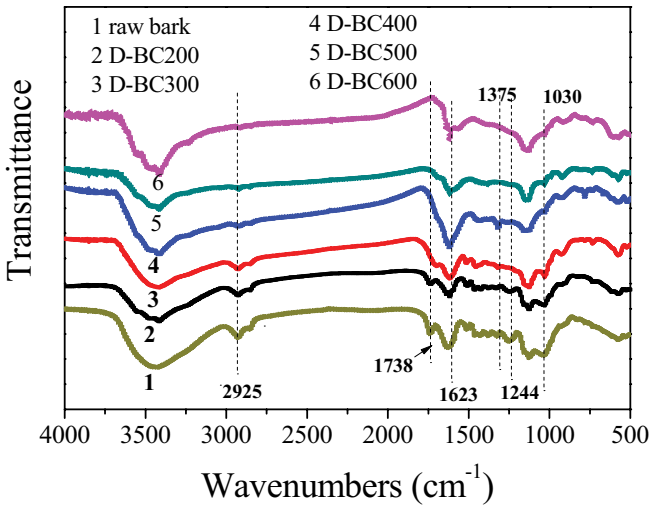

Fig. 6. FTIR spectra of the raw bark and demineralized biochar samples prepared under different pyrolytic temperatures.

and 1,030 cm^{-1} (C–O–C) almost disappeared after heating to 400°C, while the intensities at 1,623 cm^{-1} (aromatic C=C and C=O), 1375 ,cm^{-1} (CH_2) and 1,244 cm^{-1} (C–O of acetyl group) weakened simultaneously [23,31]. Usually, the increase in carbon content while decrease in oxygen content result in an obvious decrease in surface hydrophilicity (O/C ratio). We observe a reduction in surface oxygen-containing functional groups as pyrolytic temperature increases. At 1,738 cm^{-1} (C=O) the peak diminishes in intensity after heating to temperatures of 300°C and above, which implies that only the D-BC200 has comparable content of C=O functional groups with that of the raw bark. This explains the high adsorption capability of both raw bark and D-BC200 for MB removal. Surface functional groups are expected to play a key role for contaminant removal.

Using Boehm titration, the surface acidic functional groups of the raw bark and the demineralized biochar samples were quantitatively determined [20,21], as presented in Table 3. The total acidic functional groups decreased with

Table 3
Contents of surface acidic functional groups (mmol/g)

Sample	n_{RCOOH}	$n_{RCOOCOR}$	n_{ArOH}	Total acidity
Raw bark	0.267	0.289	0.385	0.941
D-BC200	0.348	0.336	0.234	0.918
D-BC400	0.522	0.265	0.055	0.842
D-BC600	0.578	0.217	0.031	0.826

Table 4
Chemical state assignments for D-BC200 and D-BC600 (%)

	C=C	C–C	C–O	CO–O
D-BC200	27.6	25.3	23.8	23.3
D-BC600	37.9	24.9	19.6	17.6

an increase in pyrolytic temperature. This is in line with the decline of O/C ratio although the reduction of the total acidity is not as significant as expected. It is worth to mention that the contents of lactonic and phenolic groups of the D-BC200 were the highest among these demineralized biochar samples. The D-BC200 and the raw bark display similar total surface acidity.

XPS is a suitable technique for studying the chemical nature of surface functional groups. Fig. 7 presents the XPS spectra of O1s, C1s and wide scan XPS spectra of the D-BC200 and D-BC600. From Fig. 7a, it is noted that the O1s intensity of D-BC200 is apparently higher than that of D-BC600, which demonstrates a higher O content in D-BC200. This is consistent with the afore-mentioned results. Generally, the asymmetric C1s XPS patterns for these two bark biochar samples can be quantitatively differentiated into four different carbon stages, including the sp^2 hybridized carbon (284.6 eV), the alcohol/ether group (C–O, about 286.2 eV), and carbonyl group (C=O, about 287.4 eV) and carboxyl acid/ester group (O–C=O, about 288.7 eV) [32,33] (Table 4). From Fig. 7d and e, both biochar samples have abundant C–O and O–C=O groups on their surface. Further, D-BC200 had a very strong photoelectron peak at around 288.7 eV, indicating the abundant existence of carboxyl acid/ester group. As we know, both C–O and O–C=O groups are associated with strong electron-donating group, which could help enhance the electron cloud of the biochar D-BC200. Therefore, the positively-charged MB molecules are expected to have a higher affinity towards the D-BC200 surface compared to that of D-BC600. From Fig. 8, both C–O and O–C=O groups had a positive correlation with the enhanced uptake of MB on D-BC200. As such, the surface functional groups of the synthesized bark biochar played the major role for the adsorptive removal of MB.

3.4. Adsorption isotherm

Isotherm study for MB adsorption on the bark biochar D-BC200 was conducted at three reaction temperatures including 288, 298 and 308 K. To provide quantitative information on the adsorption capacity, the adsorption equilibrium data at different temperatures were fitted by the Langmuir and Freundlich isotherm models, respectively. Langmuir model assumes that monolayer adsorption occurs on energetically homogeneous surface, while Freundlich isotherm assumes that a reversible adsorption happens on the energetically heterogeneous surface.

The Langmuir equation is represented as [34]:

$$q_e = \frac{q_m k_L C_e}{1 + k_L C_e} \tag{7}$$

The Freundlich equation is represented as [35]:

$$q_e = k_F C_e^{1/n} \tag{8}$$

where q_e is the amount of MB adsorbed onto BC200 (mg/g), C_e is the equilibrium concentration (mg/L), q_m is the maximum adsorption capacity of BC200 (mg/g), k_L (L/mg) is the Langmuir constant, k_F ($mg^{(1-1/n)}L^{1/n}/g$) is the Freundlich constant.

For simplicity only the isotherm at 298 K is depicted in Fig. 9. The fitted Langmuir and Freundlich isotherm parameters are listed in Table 5. Judging from Fig. 9, both Langmuir and Freundlich isotherm models present a reasonable match to the experimental data. For the as-prepared BC200, the R^2 values of Freundlich model are slightly higher than those of Langmuir model, while the R^2 values of Freundlich model are very close to those of Langmuir model for the D-BC200. At the same time, the Freundlich empirical constant, n, is within the reference range of $0.1 < 1/n < 1$, which implies a favorable adsorption of MB at all temperatures. From the Table 5, the maximal adsorption capacities achieved by the as-prepared BC200 at 288, 298 and 308 K are 178.1, 199.5, and 206.8 mg/g, respectively. For D-BC200, the maximal adsorption capacities achieved at 288, 298 and 308 K are 212.9, 237.8 and 244.8 mg/g, respectively. This shows the MB uptake increases with an increase in reaction temperatures, indicating that the adsorption process was endothermic in nature. This indicated that the adsorption capability of BC200 was quite acceptable for the practical application in water purification. The adsorption capacities of other carbonaceous sorbents reported for MB uptake in literature are compared in Table 6. The as-prepared and demineralized bark BC200 has comparable q_m values with other carbonaceous sorbents including carbon nanotubes and graphene oxide.

3.5. Thermodynamic analysis

In order to further understand the adsorption mechanism, thermodynamic parameters including standard free energy change ($\Delta G°$), standard enthalpy change ($\Delta H°$) and standard entropy change ($\Delta S°$) were calculated using the following equations:

$$\Delta G° = -RT \ln K_0 \tag{9}$$

$$\Delta G° = \Delta H° - T\Delta S° \tag{10}$$

$$\ln k_0 = -\frac{\Delta H°}{RT} + \frac{\Delta S°}{R} \tag{11}$$

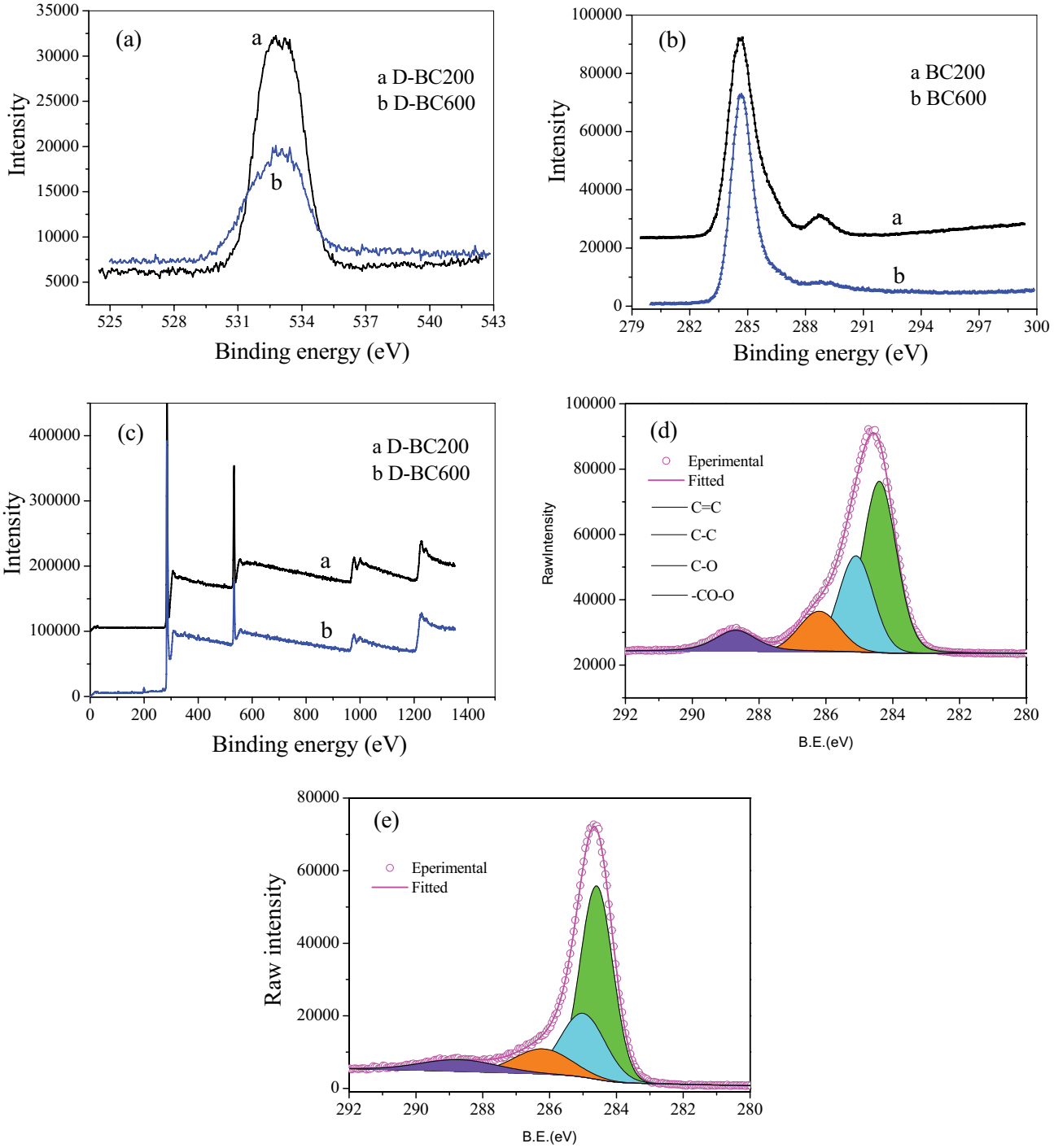

Fig. 7. XPS spectra of O1s (a), C1s (b) wide scan XPS spectra (c) of the D-BC200 and D-BC600, C1s of D-BC200 (d) and C1s of D-BC600 (e).

where the thermodynamic equilibrium constant k_0 for the adsorption process was determined by plotting $\ln q_e/C_e$ vs. q_e and extrapolating to zero q_e using a graphical method [39]. Regression straight lines were fitted through the data points by the least-squares method. The intersection with the vertical axis gives the value of $\ln k_0$ at the three different temperatures. In these equations, T is in Kelvin; $\Delta H°$ is the entropy of adsorption and R is the universal gas constant (8.314 J/mol K). The values of $\Delta H°$ and $\Delta S°$ can be obtained from the slope and intercept of a plot $\ln k_0$ vs. the reciprocal of absolute temperature (1/T).

As thermodynamic parameters listed in Table 7, under different temperatures, the negative values of $\Delta G°$ for both the D-BC200 and as-prepared BC200 suggest the spontaneous nature of MB adsorption. The enthalpy and entropy for the adsorption process using D-BC200 were found

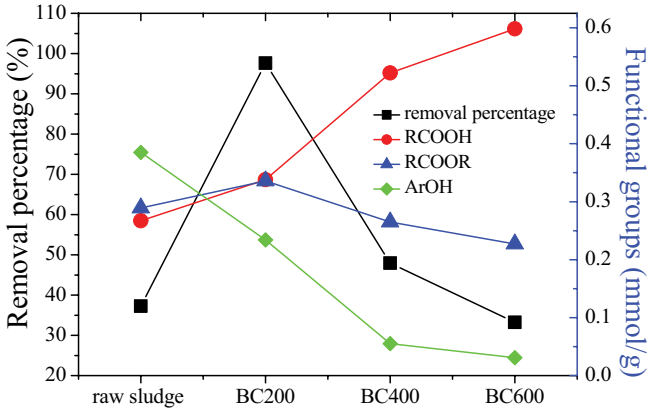

Fig. 8. Effect of surface acidic functional groups on the adsorption of MB.

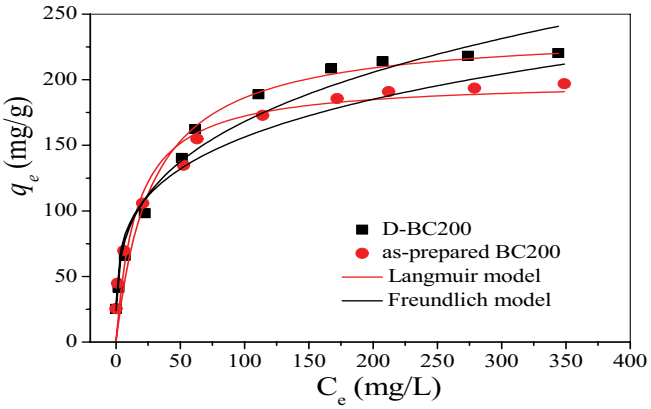

Fig. 9. Adsorption isotherms at 298 K and simulated curves by Langmuir and Freundlich models.

to be 55.63 kJ/mol and 224.8 J/mol K, respectively, while 4.58 kJ/mol and 61.0 J/mol K, respectively, for the as-prepared BC200. The positive values of the reaction enthalpy imply that the uptake of MB increase with a rise in the reaction temperature, which is consistent with the afore-mentioned results. The negative value of enthalpy change also indicated that the adsorption process is endothermic. Additionally, the enthalpy for the adsorption process using the D-BC200 was particularly higher than that using the as-prepared BC200. This demonstrates that the influence of reaction temperature on the adsorption capacity of the D-BC200 could be more significant than that on the as-prepared BC200.

3.6. Effect of co-existing anions

Coexisting anions such as nitrate, sulfate, and chloride ions (0.01 mol/L) are generally present in the wastewater stream where MB needs removal. Existence of these anions may interfere MB adsorption by competitive adsorption. The concentrations of these co-existing anions can be varied depending on referred to their actual environmental levels. Here we study the effect of co-existing anions on MB adsorption under the neutral pH condition, results are summarized in Fig. 10. It is obvious that the co-existing anions display an insignificant inhibiting effect on the removal of MB for the as-prepared BC200. The D-BC200 is a little more significantly impacted by the existence of these anions. The inorganic minerals that exist within the as-prepared BC200 may cause this key difference. They not only prevent the MB from accessing to the graphite structure of biochar but also reduce the affinity of anions to the carbon of biochar. Overall, the inhibiting effect of these co-existing anions is acceptable from a practical point of view.

4. Conclusion

Considering adsorptive removal of Methylene blue, it was observed that the bark biochar pyrolyzed at 200°C (BC200) outperformed those biochar samples produced at higher pyrolytic temperatures. For both the as-prepared and demineralized BC200, Elovich kinetic model described the adsorption process better, indicating a possible chemisorption process. The biochar particles became smaller with increasing pyrolytic temperature, with a more complex porous structure. FTIR analysis demonstrated that only the D-BC200 had comparable content of

Table 5
Langmuir and Freundlich isotherm parameters for the adsorption of MB onto the as-prepared BC200 and D-BC200

Model		Parameters	288 K	298 K	308 K
Langmuir	As-prepared BC200	q_{max} (mg/g)	178.1	199.5	206.8
		k_L (L/mg)	0.080	0.0631	0.0730
		R^2	0.924	0.939	0.934
	D-BC200	q_{max} (mg/g)	212.9	237.8	244.8
		k_L (L/mg)	0.0378	0.0362	0.0398
		R^2	0.972	0.962	0.951
Freundlich	As-prepared BC200	k_F (mg/g)	49.68	50.87	55.87
		n	4.33	4.10	4.24
		R^2	0.979	0.975	0.976
	D-BC200	k_F (mg/g)	38.5	44.1	49.6
		n	3.38	3.44	3.61
		R^2	0.952	0.968	0.976

Table 6
Comparison of MB adsorption capacities on various carbonaceous sorbents

Sorbents	q_m (mg/g)	Solution pH	References
Bark BC200	199.5	7	This study
Demineralized bark BC200	237.8	7	This study
Wheat straw BC200	46.6	7	[19]
Carbon nanotubes	188.68	6	[36]
Graphene oxide	243.9	6	[36]
Sludge biochar BC200	177.6	7	[37]
Demineralized BC200	184.9	7	[37]
Anaerobic digestion residue	9.5	N.A.	[38]
Palm bark	2.66	N.A.	[38]
Eucalyptus	2.06	N.A.	[38]
Cattle biochar	241.99	N.A.	[18]

N.A. = Not available;
Suffix of BC indicates the pyrolytic temperature for biochar.

Table 7
Values of thermodynamic parameters for MB adsorption at different temperatures

	T (K)	lnk_0	$\Delta G°$ (kJ/mol)	$\Delta H°$ (kJ/mol)	$\Delta S°$ (J/mol K)
D-BC200	288	3.628	–8.69	55.63	224.8
	298	4.943	–12.25	55.63	224.8
	308	5.149	–13.18	55.63	224.8
As-prepared	288	5.424	–13.0	4.58	61.0
BC200	298	5.509	–13.65	4.58	61.0
	308	5.549	–14.21	4.58	61.0

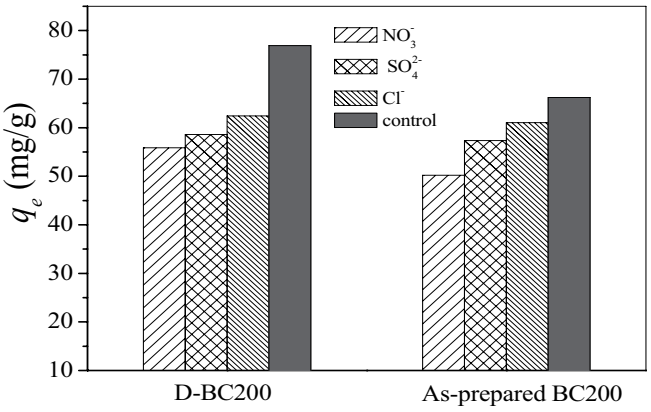

Fig. 10. Effect of co-existing anions (0.01 mol/L) on MB adsorption under neutral pH condition.

C=O functional groups with those of the raw bark. Boehm titration and XPS analysis indicated the abundant existence of carboxyl acid/ester group. The surface functional groups of synthesized bark biochar played a key role for the enhanced adsorption capability. By Langmuir isotherm model, the q_{max} on the as-prepared and demineralized BC200 achieved 199.5 and 237.8 mg/g, respectively. Thermodynamic analysis demonstrated the adsorption process was spontaneous and endothermic. The higher adsorption enthalpy indicated that the D-BC200 was more sensitive to the change of reaction temperatures.

Acknowledgement

The authors are grateful for financial support from Advanced manufacturing of biochar in UK/China/Malaysia/Nigeria (British Council, UK-China-BRI Countries Education Partnership Initiative, 2019), the National Natural Science Foundation of China (Grant no. 51378205) and the Natural Science Foundation of Henan Province (Grant No.182300410136).

References

[1] M.J. Sweetman, S. May, N. Mebberson, P. Pendleton, K. Vasilev, S.E. Plush, J.D. Hayball, Activated carbon, carbon nanotubes and graphene: materials and composites for advanced water purification, J. Carbon Res., 3 (2017) 1–29.
[2] X. Liu, M. Wang, S. Zhang, B. Pan, Application potential of carbon nanotubes in water treatment: a review, J. Environ. Sci., 25 (2013) 1263–1280.
[3] G. Ersan, O.G. Apul, F. Perreault, T. Karanfil, Adsorption of organic contaminants by graphene nanosheets: a review, Water Res., 126 (2017) 385–398.
[4] D. Woolf, J.E. Amonette, F. Alayne Street-Perrott, J. Lehmann, S. Joseph, Sustainable biochar to mitigate global climate change, Nat. Commun., 1 (2010), doi: 10.1038/ncomms1053.

[5] J.W. Lee, B. Hawkins, D.M. Day, D.C. Reicosky, Sustainability: the capacity of smokeless biomass pyrolysis for energy production, global carbon capture and sequestration, Energy Environ. Sci., 3 (2010) 1695–1705.
[6] D. Mohan, A. Sarswat, Y.S. Ok, C.U. Pittman, Organic and inorganic contaminants removal from water with biochar, a renewable, low cost and sustainable adsorbent: a critical review, Bioresour. Technol., 160 (2014) 191–202.
[7] Q. Huang, S. Song, Z. Chen, B.W. Hu, J.R. Chen, X.K. Wang, Biochar-based materials and their applications in removal of organic contaminants from wastewater: state-of-the-art review, Biochar, 1 (2019) 45–73.
[8] M. Rafatullah, O. Sulaiman, R. Hashim, A. Ahmad, Adsorption of Methylene blue on low-cost adsorbents: a review, J. Hazard. Mater., 177 (2010) 70–80.
[9] M. Ahmad, A.U. Rajapaksha, J.E. Lim, M. Zhang, N. Bolan, D. Mohan, M. Vithanage, S.S. Lee, Y.S. Ok, Biochar as a sorbent for contaminant management in soil and water: a review, Chemosphere, 99 (2014) 19–33.
[10] J.H. Qu, Research progress of novel adsorption processes in water purification, J. Environ. Sci., 20 (2008) 1–13.
[11] I. Ali, M. Asim, T.A. Khan, Low cost adsorbents for the removal of organic pollutants from wastewater, J. Environ. Manage., 113 (2012) 170–183.
[12] G.T. Li, X. Chen, L.Y. Xu, P.C. Lei, S. Zhang, C. Yang, Q.Y. Xiao, W.G. Zhao, Sonocatalytic degradation of Methylene blue using biochars derived from sugarcane bagasse, Desal. Water Treat., 88 (2017) 122–127.
[13] Z.H. Zheng, B.L. Zhao, Y.P. Guo, Y.J. Guo, T. Pak, G.T. Li, Preparation of mesoporous batatas biochar via soft-template method for high efficiency removal of tetracycline, Sci. Total Environ., 787 (2021) 147397, doi: 10.1016/j.scitotenv.2021.147397.
[14] W.S. Chen, B.L. Zhao, Y.P. Guo, Y.J. Guo, Z.H. Zheng, T. Pak, G.T. Li, Effect of hydrothermal pretreatment on pyrolyzed sludge biochars for tetracycline adsorption, J. Environ. Chem. Eng., 9 (2021) 106557, doi: 10.1016/j.jece.2021.106557.
[15] L. Leng, X. Yuan, H. Huang, J. Shao, H. Wang, X. Chen, G. Zeng, Bio-char derived from sewage sludge by liquefaction: characterization and application for dye adsorption, Appl. Surf. Sci., 346 (2015) 223–231.
[16] W. Ding, X. Dong, I.M. Ime, B. Gao, L.Q. Ma, Pyrolytic temperatures impact lead sorption mechanisms by bagasse biochars, Chemosphere, 105 (2014) 68–74.
[17] Y.S. Shen, S.L. Wang, Y.M. Tzou, Y.Y. Yan, W.H. Kuan, Removal of hexavalent Cr by coconut coir and derived chars – the effect of surface functionality, Bioresour. Technol., 104 (2012) 165–172.
[18] Y. Zhu, B.J. Yi, Q.X. Yuan, Y.L. Wu, M. Wang, S.P. Yan, Removal of Methylene blue from aqueous solution by cattle manure-derived low temperature biochar, RSC Adv., 8 (2018) 19917–19929.
[19] G.T. Li, W.Y. Zhu, C.Y. Zhang, S. Zhang, L.L. Liu, L.F. Zhu, W.G. Zhao, Effect of a magnetic field on the adsorptive removal of Methylene blue onto wheat straw biochar, Bioresour. Technol., 206 (2016) 16–22.
[20] M. Abdulkarim, A.A. Fahmi, Adsorption of lead ions from aqueous solutions on activated carbon and chemically modified activated carbon prepared from date pits, Adsorpt. Sci. Technol., 22 (2004) 119–34.
[21] V. Strelko, D.J. Malik, M. Streat, Characterization of the surface of oxidized carbon adsorbents, Carbon, 40 (2002) 95–104.
[22] M.D. Inyang, B. Gao, Y. Yao, Y.W. Xue, R.Z. Andrew, P. Pratap, X.D. Cao, Removal of heavy metals from aqueous solution by biochars derived from anaerobically digested biomass, Bioresour. Technol., 110 (2012) 50–56.
[23] B.L. Chen, Z.M. Chen, Sorption of naphthalene and 1-naphthol by biochars of orange peels with different pyrolytic temperatures, Chemosphere, 76 (2009) 127–133.
[24] S. Lagergren, Zur theorie der sogenannten adsorption gelöster stoffe. Kungliga Svenska Vetenskapsakademiens, Handlinga, 24 (1898) 1–39.
[25] Y.S. Ho, G. McKay, Pseudo-second-order model for sorption process, Process Biochem., 34 (1999) 451–465.
[26] M. Kithome, J.W. Paul, L.M. Lavkulich, A.A. Bomke, Kinetics of ammonium adsorption and desorption by the natural zeolite clinoptilolite, Soil Sci. Soc. Am., 62 (1988) 622–629.
[27] C.W. Cheung, J.F. Porter, G. Mckay, Sorption kinetics for the removal of copper and zinc from effluents using bone char, Sep. Purif. Technol., 19 (2000) 55–64.
[28] C. Aharoni, D.L. Sparks, S. Levinson, I. Revina, Kinetics of soil chemical reactions: relationships between empirical equations and diffusion models, Soil Sci. Soc. Am. J., 55 (1991) 1307–1312.
[29] A. Pavlatou, N.A. Polyzopouls, The role of diffusion in the kinetics of phosphate desorption: the relevance of the Elovich equation, Eur. J. Soil Sci., 39 (1988) 425–436.
[30] X. Chen, G. Chen, L. Chen, Y. Chen, J. Lehmann, M.B. McBride, A.G. Hay, Adsorption of copper and zinc by biochars produced from pyrolysis of hardwood and corn straw in aqueous solution, Bioresour. Technol., 102 (2011) 8877–8884.
[31] X.D. Zhu, Y.C. Liu, C. Zhou, G. Luo, S.C. Zhang, J.M. Chen, A novel porous carbon derived from hydrothermal carbon for efficient adsorption of tetracycline, Carbon, 77 (2014) 627–636.
[32] S. Altenor, B. Carene, E. Emmanuel, J. Lambert, J. Ehrhardt, S. Gaspard, Adsorption studies of Methylene blue and phenol onto vetiver roots activated carbon prepared by chemical activation, J. Hazard. Mater., 165 (2009) 1029–1039.
[33] M. Pumera, B. Smid, K. Veltruska, Influence of nitric acid treatment of carbon nanotubes on their physico-chemical properties, J. Nanosci. Nanotechnol., 9 (2009) 2671–2676.
[34] I. Langmuir, Kinetic model for the sorption of dye aqueous solution by clay-wood sawdust mixture, J. Am. Chem. Soc., 38 (1916) 2221–2295.
[35] H.M.F. Freundlich, Uber die adsorption in lasungen, J. Phys. Chem., 57 (1906) 385–470.
[36] Y.H. Li, Q.J. Du, T.H. Liu, X.J. Peng, J.J. Wang, J.K. Sun, Y.H. Wang, S.L. Wu, Z.H. Wang, Y.Z. Xia, L.H. Xia, Comparative study of Methylene blue dye adsorption onto activated carbon, graphene oxide, and carbon nanotubes, Chem. Eng. Res. Des., 91 (2013) 361–368.
[37] W.S. Chen, Y.P. Guo, X. Mi, Y. Yu, G.T. Li, Enhanced adsorptive removal of Methylene blue by low-temperature biochar derived from municipal activated sludge, Desal. Water Treat., 188 (2020) 257–265.
[38] L. Sun, S.G. Wan, W.S. Luo, Biochars prepared from anaerobic digestion residue, palm bark, and eucalyptus for adsorption of cationic Methylene blue dye: characterization, equilibrium, and kinetic studies, Bioresour. Technol., 140 (2013) 406–413.
[39] X. Yuan, W. Xing, S.P. Zhuo, Z.H. Han, G.Q. Wang, X.L. Gao, Z.F. Yan, Preparation and application of mesoporous Fe/carbon composites as a drug carrier, Microporous Mesoporous Mater., 117 (2009) 678–684.